ACS Chemical Neuroscience

Letter

pubs.acs.org/chemneuro

PET Neuroimaging Studies of [^{18}F]CABS13 in a Double Transgenic Mouse Model of Alzheimer's Disease and Nonhuman Primates

Steven H. Liang,[†,‡] Jason P. Holland,[‡] Nickeisha A. Stephenson,[†,‡] Alina Kassenbrock,[†] Benjamin H. Rotstein,[†,‡] Cory P. Daignault,[†] Rebecca Lewis,[†] Lee Collier,[†,‡,§] Jacob M. Hooker,[‡,∥] and Neil Vasdev*[,†,‡]

[†]Division of Nuclear Medicine and Molecular Imaging & Center for Advanced Medical Imaging Sciences, Massachusetts General Hospital, Boston, Massachusetts 02114, United States

[‡]Department of Radiology, Harvard Medical School, Boston, Massachusetts 02114, United States

[§]Advion, Inc., Ithaca, New York 14850, United States

[∥]Athinoula A. Martinos Center for Biomedical Imaging, Massachusetts General Hospital, Charlestown, Massachusetts 02129, United States

Supporting Information

ABSTRACT: Fluorine-18 labeled 2-fluoro-8-hydroxyquinoline ([^{18}F]CABS13) is a promising positron emission tomography (PET) radiopharmaceutical based on a metal chelator developed to probe the "metal hypothesis of Alzheimer's disease". Herein, a practical radiosynthesis of [^{18}F]CABS13 was achieved by radiofluorination followed by deprotection of an *O*-benzyloxymethyl group. Automated production and formulation of [^{18}F]CABS13 resulted in 19 ± 5% uncorrected radiochemical yield, relative to starting [^{18}F]fluoride, with ≥95% chemical and radiochemical purities, and high specific activity (>2.5 Ci/μmol) within 80 min. Temporal PET neuroimaging studies were carried out in female transgenic B6C3-Tg(APPswe,PSEN 1dE9)85Dbo/J (APP/PS1) and age-matched wild-type (WT) B6C3F1/J control mice at 3, 7, and 10 months of age. [^{18}F]CABS13 showed an overall higher uptake and retention of radioactivity in the central nervous system of APP/PS1 mice versus WT mice with increasing age. However, PET/magnetic resonance imaging in normal nonhuman primates revealed that the tracer had low uptake in the brain and rapid formation of a hydrophilic radiometabolite. Identification of more metabolically stable ^{18}F-hydroxyquinolines that can be readily accessed by the radiochemical strategy presented herein is underway.

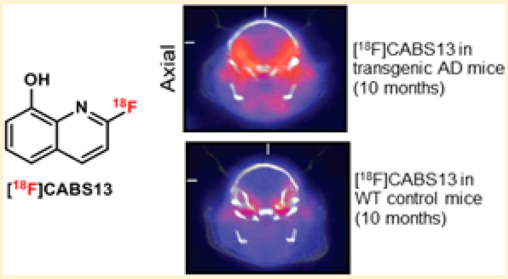

KEYWORDS: *[^{18}F]CABS13, metal hypothesis of Alzheimer's disease, rodents, nonhuman primates, transgenic mice, APP/PS1*

Detection of amyloid-beta protein aggregates (Aβ plaques) in brain tissues with positron emission tomography (PET) is an intense area of clinical research for Alzheimer's disease (AD) and related dementias.[1] Several PET radiopharmaceuticals have been developed to interrogate Aβ plaques, including 2-(4′-[^{11}C]methylaminophenyl)-6-hydroxybenzothiazole (^{11}C-Pittsburgh Compound B; [^{11}C]PiB) and 2-(2-[^{18}F]fluoro-6-(methylamino)pyridin-3-yl)benzofuran-5-ol ([^{18}F]NAV4694; [^{18}F]AZD4694), and three tracers have recently been approved for use in patients with cognitive impairment by the United States Food and Drug Administration: (*E*)-4-(2-(6-(2-(2-(2-[^{18}F]fluoroethoxy)ethoxy)ethoxy)pyridin-3-yl)vinyl)-*N*-methyl benzenamine ([^{18}F]Florbetapir), 2-(3-[^{18}F]fluoro-4-(methylamino)phenyl)-1,3-benzothiazol-6-ol ([^{18}F]Flutametamol), and 4-(*E*)-(2-(4-(2-(2-(2-[^{18}F]fluoroethoxy)ethoxy)ethoxy)phenyl)vinyl)-*N*-methylaniline ([^{18}F]Florbetaben).[2] Although clinical trials have been realized with the above-mentioned radiopharmaceuticals, these agents are still under further development to study their sensitivity to low levels of Aβ,[3] as well as to explore the correlation of memory decline in healthy subjects and patients with early mild cognitive impairment.[4] Furthermore, recent failures of numerous anti-amyloid therapies in the final stages of clinical testing have raised questions about the value and purported specificity of Aβ imaging with the existing PET radiopharmaceuticals.[3] New radiotracers for specific Aβ quantification are desperately needed, not only as early detection diagnostics but also to enable accurate classification of subjects for clinical trials and to assess therapeutic response.[5]

The "metal hypothesis of AD"[6−11] stems from a complex and growing body of evidence showing that various metal ions promote Aβ aggregation from the stage of oligomer formation, in addition to playing critical physiological roles in normal synaptic transmission and neuronal survival. In particular, Aβ has Zn and Cu binding sites and these metal ions are enriched in Aβ aggregates in transgenic AD mice as well as in patients, as attributed to insufficient metal reuptake.[12−14] It is known that Zn, Cu, and Fe ions are involved in the Aβ deposition and

Published: March 17, 2015

DOI: 10.1021/acschemneuro.5b00055
ACS Chem. Neurosci. 2015, 6, 535−541

Scheme 1. Improved Radiosynthesis of [^{18}F]CABS13 Based on Benzyloxymethyl Precursor 1[a]

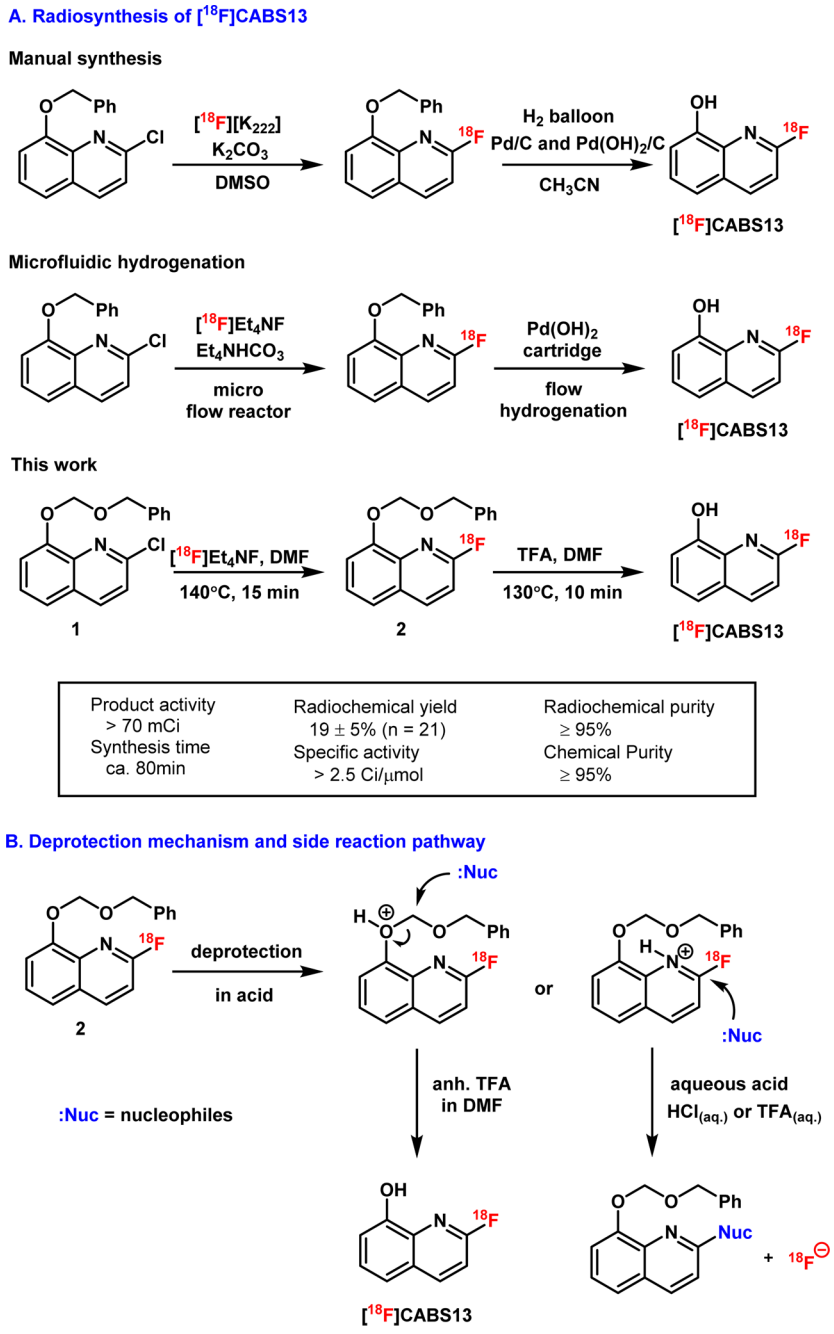

[a](A) Reaction conditions and radiosynthesis results. (B) Plausible mechanism of trifluoroacetic acid mediated deprotection and formation of side products under aqueous acidic conditions.

stabilization, and metal chelating agents can facilitate dissolution of Aβ deposits by preventing metal−Aβ interaction,[15] thereby representing both therapeutic and diagnostic strategies for AD and related dementias.[16−20] Development of a single-photon emission computed tomography (SPECT) or PET radiotracer based on a recognized metal chelator could advance our understanding of neurological disorders that are affected by dysregulation of metal functions, and may prove useful in monitoring therapy for patients with neurodegenerative diseases.

A prototypical hydroxyquinoline-based drug, clioquinol (5-chloro-7-iodo-8-hydroxyquinoline; CQ), prevents Aβ toxicity in vitro and out-competes Aβ for metal ions without changing the activity of Zn/Cu-dependent enzymes.[15,21] Further investigations revealed that CQ not only prevents or reverses extracellular Aβ aggregation, but also transports metal ions across cell membranes to increase intracellular metal concentration, thereby initiating protective cell signaling.[5,13] These efforts stimulated the development of radiolabeled CQ and its derivatives for molecular imaging studies. An early attempt to use [^{123}I]CQ as an imaging marker via SPECT failed due to low brain uptake in preclinical and clinical research.[22,23] Our laboratory discovered the first PET radiotracer to probe the metal hypothesis of AD, namely, [^{18}F]2-fluoro-8-hydroxyquinoline ([^{18}F]CABS13), and carried out a promising preliminary PET imaging study in a transgenic mouse model of AD in aged

DOI: 10.1021/acschemneuro.5b00055
ACS Chem. Neurosci. 2015, 6, 535−541

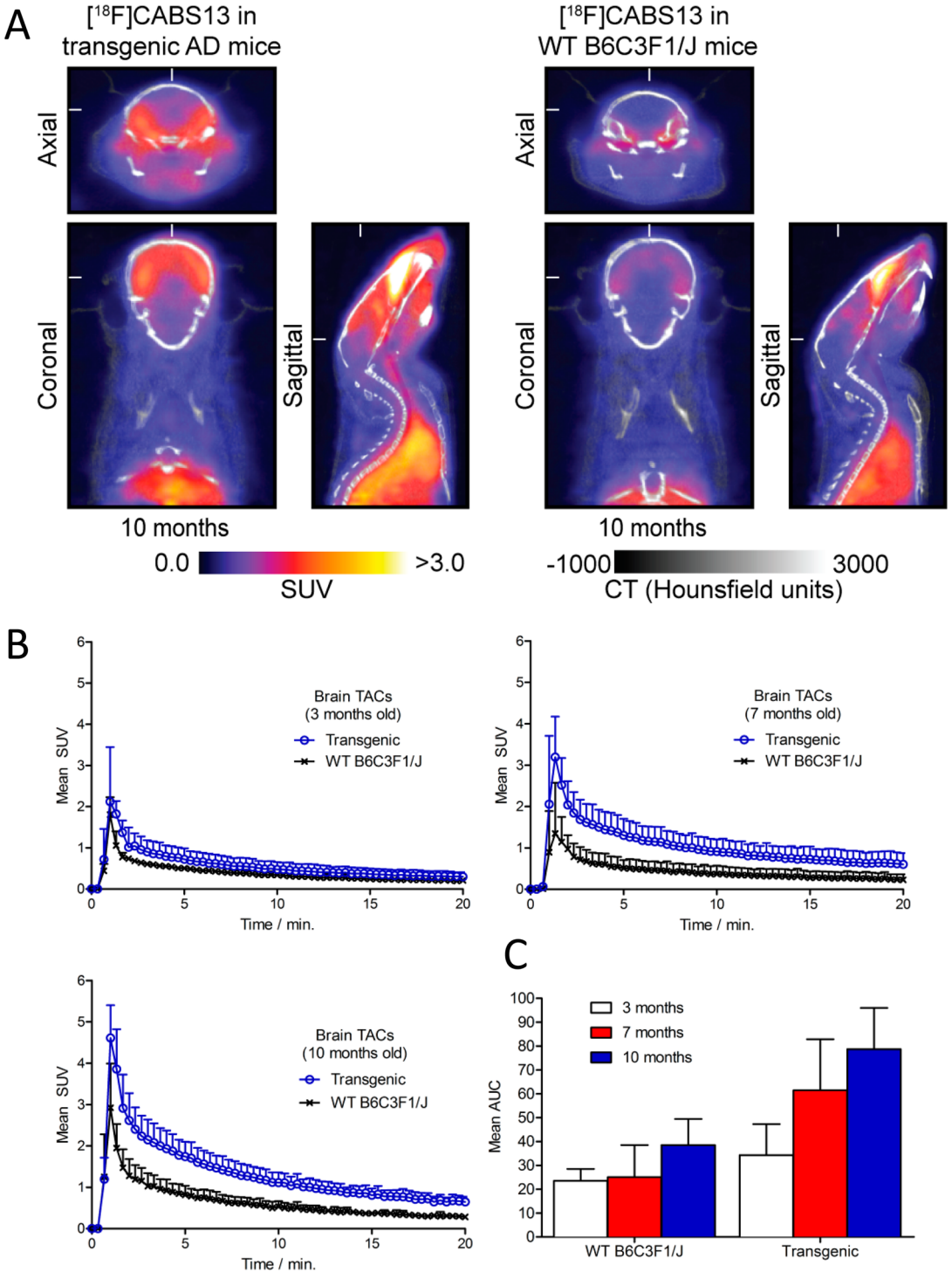

Figure 1. Longitudinal PET studies in APP/PS1 transgenic mice of AD versus wild-type controls. (A) PET images (axial, coronal, and sagittal) summed at 5−10 min postinjection of 10 month-old transgenic mice (left) versus WT controls (right). (B) Time−activity curves and (C) AUC measurement in whole brain between transgenic mice of AD versus WT controls in 3, 7, and 10 months.

rodents with well-developed plaque formation (10−12 months).[24] It is noteworthy that exploration of the "metal hypothesis of AD" with PET is actively pursued by several laboratories, with recent accounts of carbon-11 and fluorine-18 labeled analogues of L2-b (N^1,N^1-dimethyl-N^4-(pyridin-2-ylmethyl)benzene-1,4-diamine)[25] and copper-64-labeled bis(-thiosemicarbazonato)Cu^{II}complexes.[26,27]

While our preliminary studies showed that [^{18}F]CABS13 may be promising for imaging Aβ plaques in vivo, the lack of a facile and automated radiosynthesis for this tracer and related hydroxyquinolines has hindered further development. Scheme 1A shows our original synthesis of [^{18}F]CABS13 which employed a palladium-catalyzed hydrogenation for mild deprotection of an *O*-benzyl protecting group following radiofluorination (manual synthesis),[24] and our recently adapted automated process using a flow radiofluorination and flow hydrogenation devices (microfluidic hydrogenation).[28] Herein we describe a novel radiosynthetic strategy for the facile

DOI: 10.1021/acschemneuro.5b00055
ACS Chem. Neurosci. 2015, 6, 535−541

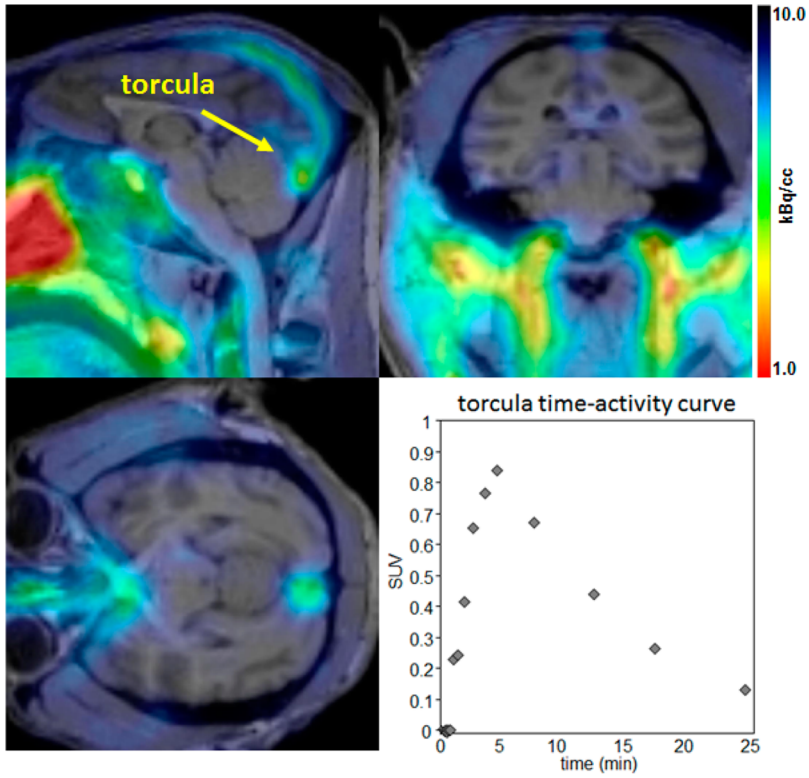

Figure 2. Summed PET (0−15 min) with structural MR images (top). Radioactivity is seen primarily in the confluence of the sinuses (torcula) with the highest intensity just inside the occipital protuberance (lower left). Time−activity curve for the radioactivity observed is also shown (bottom right).

preparation of [^{18}F]CABS13, longitudinal PET-CT imaging studies in a double transgenic mouse model of AD spanning from early to mature plaque stages, and PET/magnetic resonance (MR) imaging in healthy *Papio anubis* baboons.

RESULTS AND DISCUSSION

As shown in Scheme 1A, a synthesis of [^{18}F]CABS13 was carried out by reaction of [^{18}F]NEt$_4$F with a novel benzyloxy methyl (BOM) protected precursor **1**, followed by a trifluoroacetic acid (TFA) mediated deprotection. The radiosynthesis of [^{18}F]CABS13 was automated using a commercial radiofluorination device (GE Tracerlab FX$_{F-N}$) in an uncorrected radiochemical yield of 19 ± 5%, relative to starting [^{18}F] fluoride, with high chemical and radiochemical purities (both ≥95%) as well as high specific activity (>2.5 Ci/μmol). The product was formulated in 10% ethanol in saline solution and no radiolysis was detected over 6 h. Greater than 50% increase of radiochemical yield and more than 2-fold increase in specific activities were achieved compared with our original method to synthesize [^{18}F]CABS13.[24]

The reaction underwent an activation step via coordination to phenolic oxygen, followed by deprotection in situ (Scheme 1B, route A) at elevated temperature (see the Supporting Information). When aqueous acids were used, an interfering pathway decomposed the desired ^{18}F-labeled hydroxyquinoline. Specifically, a nucleophile from the reaction mixture was found to displace the ^{18}F-fluorine at the 2-position of the pyridine, thereby generating nonradioactive byproducts and free fluoride (Scheme 1B, route B). Such undesirable side-reactions could become a major hurdle to removing protecting groups in molecules bearing 2-[^{18}F]fluoropyridine moieties, which are widely used building blocks, and can be problematic toward other functional groups that may undergo acid-catalyzed nucleophilic displacement reactions. Notably, the di-*t*-butyloxycarbonyl (Boc) protected precursor was not stable under basic labeling conditions and provided inferior radiochemical conversions, compared to **1**. The utilization of the *O*-BOM group was effective and can be easily removed under anhydrous acidic conditions, thereby obviating the need of either manual synthesis or specialized devices to prepare [^{18}F]CABS13.[24,28] This method also provides an alternative protection/deprotection method for radiotracer design and should prove to be broadly applicable for synthesis of hydroxyquinolines and related scaffolds.

Dynamic PET/CT imaging was carried out to investigate temporal differences in [^{18}F]CABS13 binding in double transgenic (APP/PS1) mice at ages 3, 7, and 10 months along with age-matched wild-type controls (WT; B6C3F1/J) (Figure 1). Axial, coronal, and sagittal images of the murine brains summed from 5−10 min postinjection of [^{18}F]CABS13 are presented in Figure 1A. As predicted, increased uptake and retention of radiotracer binding was observed in the whole brains of transgenic mice compared with WT controls. The time−activity curves revealed a similar trend of increased brain penetration with increasingly higher brain uptake at 3, 7, and 10 months for both groups of mice (Figure 1B). Maximum uptake (whole brain peak uptake SUV(mean) = 2.2, 3.2 and 4.6, in transgenic mice and 1.8, 1.4, and 2.9 for WT controls at 3, 7, and 10 months, respectively) was observed in both genotypes after 1 min postinjection of the radiotracer, followed by a relatively slow washout in the transgenic mice and a more rapid washout in WT mice as the radioactivity cleared from normal tissues. A comparison of the area under the curve (AUC) analysis (Figure 1C) over time for the respected genotypes

DOI: 10.1021/acschemneuro.5b00055
ACS Chem. Neurosci. 2015, 6, 535−541

underscores the trends observed in the TACs. In addition to our preliminary study on well-developed AD mice (10−12 months),[24] the temporal PET/CT imaging studies from early to well-developed stages (3−10 months) with [^{18}F]CABS13 in transgenic mouse models of AD presented herein provides further and consistent evidence for a PET tracer with potential to probe the "metal hypothesis of AD".

Encouraged by the temporal PET imaging of [^{18}F]CABS13 in rodent models, we carried out preliminary PET/MR imaging studies in normal baboons. Analysis of the PET/MR imaging data reveals that radioactivity enters the cranium and is observed in the torcula reaching a maximum at approximately 5 min post injection of the radiotracer (Figure 2). Over time ($t_{1/2}$ ∼ 5 min), the radioactivity distributes to the superior sagittal, occipital, and transverse sinuses. A very small proportion of the radioactivity at these early time points appears in the brain; however, it is difficult to determine if the activity observed represents the blood pool uptake within the brain. A second imaging study was carried out with arterial plasma analysis, and was consistent with the previous scan. The time−activity curve of radioactivity in the plasma is well matched to that derived from a region of interest placed in the torcula as would be expected. Further analysis of the radioactivity in arterial plasma suggests that the majority (>90%) of circulating radioactivity at 5 min post administration of the radiotracer is a polar radiometabolite which is unlikely free [^{18}F]fluoride because of the absence of noted uptake in bone regions. Although specific binding and metabolism (potentially attributed to sulfation and/or glucuronidation) may be different in higher species, given the fast metabolism and low retention of [^{18}F]CABS13 in the nonhuman primate brain, this ^{18}F-labeled hydroxyquinoline was not further evaluated.

In summary, we demonstrated a novel high-yielding radiosynthetic method to prepare [^{18}F]CABS13 employing benzyloxymethyl as a handle for protection and deprotection of a phenolic functionality under metal-free anhydrous conditions. Despite the increased radiotracer retention in the brains of APP/PS1 mice over time, rapid metabolism and low brain penetration observed in the nonhuman primate imaging studies will preclude its further use. The radiosynthetic strategy developed herein represents the effective use of a BOM protecting group to eliminate the need for hazardous transition-metal mediated hydrogenations in radiochemistry, enabled facile automation, and should be broadly applicable for the synthesis of radiolabeled hydroxyquinolines and related scaffolds. Our current efforts will take advantage of protection/deprotection strategy and will be directed toward radiolabeling either at the nonactivated aromatic phenolic moiety via our recently described hypervalent iodonium ylide method for radiofluorination of electron-rich aromatic rings,[29] or at the aliphatic alkyl chain based on 5,7-dichloro-2-(dimethylamino)methyl-8-quinolinol (PBT2),[20] a newer generation hydroxyquinoline based metal chelator in phase II clinical trials.

METHODS

Synthesis of [^{18}F]CABS13. Detailed procedures of precursor synthesis are provided in the Supporting Information. The radiofluorination was carried out between precursor **1** (6 mg in 1.1 mL DMF) and [^{18}F]Et_4NF (prepared with tetraethylammonium bicarbonate (14 mg) and aqueous [^{18}F]fluoride, coevaporated with CH_3CN three times) at 140 °C for 15 min to yield ^{18}F-labeled compound **2**. The deprotection reactions were tested in various acidic conditions at different temperatures in order to identify the optimal conditions for the synthesis of [^{18}F]CABS13. Radiochemical conversion yields were determined by radio-TLC and the identity of the molecule was confirmed by radio-HPLC. The optimized reaction parameters were selected for automated synthesis of [^{18}F]CABS13. Detailed procedures are provided in the Supporting Information. Analyses of radioactive mixtures were performed by HPLC with an in-line UV (λ = 254 nm) detector in series with a CsI pin diode radioactivity detector. To determine the identity of [^{18}F]CABS13, aliquots of the formulated product were injected onto an analytical HPLC system using an analytical Luna C-18 column (150 × 4.6 mm, 5 μm) and eluted with mobile phase (CH_3CN/0.1N ammonium formate, 70:30 v/v) with a flow rate of 1 mL/min, monitored at λ = 254 nm. The major radiochemical product was identified as [^{18}F]CABS13 (t_R = ∼5.8 min). A mass calibration curve (λ = 254 nm) was generated from known concentrations of CABS13 in solutions to determine the specific activity.

PET Imaging Studies in APP/PS1 and Wild-Type Control Mice. All animal experiments were conducted in compliance with Institutional Animal Care and Use Committee (IACUC) guidelines and the *Guide for the Care and Use of Laboratory Animals*. Female, wild-type B6C3F1/J mice (6−8 weeks old) and transgenic B6C3-Tg(APPswe,PSEN 1dE9)85Dbo/J (APP/PS1; Stock No.: 034829-JAX or MMRRC No. 034) mice were obtained from Jackson Laboratory (Bar Harbor, ME). Mice were provided with food and water ad libitum and were allowed to acclimatize for 1 month prior to conducting PET/CT and biodistribution experiments. Dynamic PET/CT imaging experiments were conducted on a dedicated small-animal PET/CT scanner (eXplore Vista-CT, Sedecal, Algete, Spain) equipped with VISTA-CT version 4.11 software. In separate studies (n = 3), mice were administered formulations of [^{18}F]CABS13 (∼4.0−16.0 MBq [∼100−432 μCi], specific activity of >2 Ci/μmol, in 200 μL sterile PBS, pH 7.4, ≤5% v/v EtOH) via intravenous (iv) tail vein injection using a catheter. Approximately 5 min prior to recording PET images, mice were anesthetized by inhalation of 3−4% isoflurane (Baxter Healthcare, Deerfield, IL)/oxygen gas mixture, and a catheter was inserted into the tail vein, and then mice were transferred to the scanner bed and placed in the prone position. Anesthesia was maintained with 1−2% isoflurane/oxygen gas mixture (flow rate ∼ 5 L/min). Coregistered dynamic PET/CT images were recorded for a total of 20−30 min postinjection radiotracer injection ($n \geq 3$ mice/time point). List-mode data were acquired for 20−30 min per scan using a γ-ray energy window of 250−700 keV. To ensure that the activity bolus was measured, PET/CT data acquisition was initiated 20 s prior to injecting the radioactivity. Data were processed by three-dimensional Fourier rebinning (3D-FORE), and images were reconstructed using the two-dimensional ordered-subset expectation maximum (2D-OSEM) algorithm. Image data were normalized to correct for nonuniformity of response of the PET, dead-time count losses, positron branching ratio, and physical decay to the time of injection, but no attenuation, scatter, or partial-volume averaging correction was applied. An empirically determined system calibration factor (in units of Bq/cps) combined with the decay corrected administered activity and the animal weight were used to parametrize image activity in terms of the standardized uptake value (SUV). Manually drawn 2D regions of interest (ROIs) or 3D volumes of interest (VOIs) were used to determine the maximum and mean SUV radiotracer uptake in various tissues. Time-activity curves (TACs) were generated from ROI analysis on dynamic PET/CT data using 20 s frames. CT images were recorded using an X-ray current of 300 μA, 360 projections, and an image size of 63.8 mm × 63.8 mm × 46.0 mm. Data were acquired using the Vista CT 4.11 Build 701 software, and reconstructed images were analyzed by using VivoQuant 1.23 (InviCRO, LLC, Boston, MA). Data and statistical analyses were performed using GraphPad Prism 5.01 (GraphPad Software, Inc., La Jolla, CA) and Microsoft Excel.

PET Imaging Studies in Nonhuman Primates. One adult baboon (Papio Anubis, female, 5 y.o., 14.1 kg), deprived of food for 12 h prior to imaging experiments, was included in the study (n = 2). Intramuscular ketamine (10 mg/kg) was administered for animal

DOI: 10.1021/acschemneuro.5b00055
ACS Chem. Neurosci. 2015, 6, 535−541

preparation and intubation. The animal was catheterized antecubitally for hydration and radiotracer injection. In one experiment, a radial arterial line was placed for plasma and metabolite analysis. For maintenance of anesthesia throughout the imaging study, the baboon was provided 1−1.5% isoflurane (Forane) in a mixture of medical oxygen and nitrogen. Body temperature was maintained by heated water blanket. Vital signs including end tidal CO_2, SpO_2, heart rate, respiration rate, and blood pressure were monitored and maintained within normal ranges during the studies. PET and MRI images were acquired on a 3T Siemens TIM-Trio with a BrainPET insert (Siemens, Erlangen, Germany). A custom PET/MRI compatible eight-channel array coil for nonhuman primate brain imaging was used to improve image signal and quality. Dynamic PET image acquisition was initiated concurrently with the administration of the radiotracer (5 ± 0.2 mCi, 2 scans) in a homogeneous solution of 10% ethanol and 90% isotonic saline, and continued for duration of 120 min. A high-resolution anatomical scan using multiecho MPRAGE sequence (TR = 2530 ms, TE1/TE2/TE3/TE4 = 1.64/3.5/5.36/7.22 ms, TI = 1200 ms, flip angle = 7°, and 1 mm isotropic) was acquired for anatomic coregistration. Blood sampling from the radial arterial line occurred nominally every 10 s for the first 3 min (∼1 mL each) after radiotracer administration, followed by sampling at 5, 10, 20, 30, 45, 60, and 90 min time points (∼3 mL each) for plasma and metabolite analysis. Arterial samples were centrifuged to obtain plasma, which was then removed and placed in an automated gamma counter that was calibrated with the PET scanner and using a 350−600 keV window. Beginning with the arterial sample acquired at 5 min after radiotracer administration, an aliquot (300 μL) of plasma was added to acetonitrile (300 μL) and centrifuged for 1−2 min to obtain protein-free plasma (PFP). An aliquot (300 μL) of PFP was diluted with deionized water (2 mL), and loaded onto a customized automated robot, fitted with Phenomenex Strata-X 500 mg SPE cartridges that were primed with ethanol (2 mL) and deionized water (20 mL). Solutions of PFP were loaded on SPE cartridges, and then extracted sequentially with 4 mL of 100% 0.1 N ammonium formation (AMF); 10% CH_3CN/0.1N AMF; 20% CH_3CN/0.1N AMF; 30% CH_3CN/0.1N AMF; 40% CH_3CN/0.1N AMF; 70% CH_3CN/0.1N AMF; 100% CH_3CN. This program had been previously tested with [^{18}F]CABS13 to determine its retention properties. Each eluent sample was counted in an automated gamma counter to determine the presence of radiolabeled metabolites.

■ ASSOCIATED CONTENT

Ⓢ Supporting Information

Synthesis of precursors, automated radiosynthesis, and small animal PET imaging studies of [^{18}F]CABS13 in mice and nonhuman primates. This material is available free of charge via the Internet at http://pubs.acs.org.

■ AUTHOR INFORMATION

Corresponding Author

*Tel: 617-643-4736. Fax: 617-726-6165. E-mail: vasdev.neil@mgh.harvard.edu.

Author Contributions

The manuscript was written through contributions of all listing authors. All authors have discussed and approved the final version of the manuscript.

Funding

We thank the Australian National Science and Technology Organisation for partial financial support.

Notes

The authors declare no competing financial interest.

■ ACKNOWLEDGMENTS

We thank the Massachusetts General Hospital PET Core facility for ^{18}F-fluoride production as well as Dr. Ivan Greguric.

■ REFERENCES

(1) Zhu, L., Ploessl, K., and Kung, H. F. (2014) PET/SPECT Imaging Agents for Neurodegenerative Diseases. *Chem. Soc. Rev. 43*, 6683−6691.

(2) McConathy, J., and Sheline, Y. I. (2014) Imaging Biomarkers Associated With Cognitive Decline: A Review. *Biol. Psychiatry*, DOI: 10.1016/j.biopsych.2014.08.024.

(3) Kepe, V., Moghbel, M. C., Langstrom, B., Zaidi, H., Vinters, H. V., Huang, S.-C., Satyamurthy, N., Doudet, D., Mishani, E., Cohen, R. M., Hoilund-Carlsen, P. F., Alavi, A., and Barrio, J. R. (2013) Amyloid-β Positron Emission Tomography Imaging Probes: A Critical Review. *J. Alzheimer's Dis. 36*, 613−631.

(4) Villemagne, V. L., Burnham, S., Bourgeat, P., Brown, B., Ellis, K. A., Salvado, O., Szoeke, C., Macaulay, S. L., Martins, R., Maruff, P., Ames, D., Rowe, C. C., and Masters, C. L. (2013) Amyloid β Deposition, Neurodegeneration, and Cognitive Decline in Sporadic Alzheimer's Disease: A Prospective Cohort Study. *Lancet Neurol. 12*, 357−367.

(5) Holland, J. P., Liang, S. H., Rotstein, B. H., Collier, T. L., Stephenson, N. A., Greguric, I., and Vasdev, N. (2014) Alternative Approaches for PET Radiotracer Development in Alzheimer's Disease: Imaging beyond Plaque. *J. Labelled Compd. Radiopharm. 57*, 323−331.

(6) Crouch, P. J., and Barnham, K. J. (2012) Therapeutic Redistribution of Metal Ions To Treat Alzheimer's Disease. *Acc. Chem. Res. 45*, 1604−1611.

(7) Frederickson, C. J., Koh, J.-Y., and Bush, A. I. (2005) The Neurobiology of Zinc in Health and Disease. *Nat. Rev. Neurosci. 6*, 449−462.

(8) Watt, N. T., Whitehouse, I. J., and Hooper, N. M. (2011) The Role of Zinc in Alzheimer's Disease. *Int. J. Alzheimer's Dis.*, 971021.

(9) Bush, A. I. (2008) Drug Development Based on the Metals Hypothesis of Alzheimer's Disease. *J. Alzheimer's Dis. 15*, 223−240.

(10) Bush, A. I., and Tanzi, R. E. (2008) Therapeutics for Alzheimer's Disease Based on the Metal Hypothesis. *Neurotherapeutics 5*, 421−432.

(11) Savelieff, M. G., Lee, S., Liu, Y., and Lim, M. H. (2013) Untangling Amyloid-β, Tau, and Metals in Alzheimer's Disease. *ACS Chem. Biol. 8*, 856−865.

(12) Lee, J.-Y., Mook-Jung, I., and Koh, J.-Y. (1999) Histochemically Reactive Zinc in Plaques of the Swedish Mutant β-Amyloid Precursor Protein Transgenic Mice. *J. Neurosci. 19*, RC10.

(13) Lovell, M. A., Robertson, J. D., Teesdale, W. J., Campbell, J. L., and Markesbery, W. R. (1998) Copper, Iron and Zinc in Alzheimer's Disease Senile Plaques. *J. Neurol. Sci. 158*, 47−52.

(14) Suh, S. W., Jensen, K. B., Jensen, M. S., Silva, D. S., Kesslak, P. J., Danscher, G., and Frederickson, C. J. (2000) Histochemically-Reactive Zinc in Amyloid Plaques, Angiopathy, and Degenerating Neurons of Alzheimer's Diseased Brains. *Brain Res. 852*, 274−278.

(15) Cherny, R. A., Atwood, C. S., Xilinas, M. E., Gray, D. N., Jones, W. D., McLean, C. A., Barnham, K. J., Volitakis, I., Fraser, F. W., Kim, Y.-S., Huang, X., Goldstein, L. E., Moir, R. D., Lim, J. T., Beyreuther, K., Zheng, H., Tanzi, R. E., Masters, C. L., and Bush, A. I. (2001) Treatment with a Copper-Zinc Chelator Markedly and Rapidly Inhibits Aβ-Amyloid Accumulation in Alzheimer's Disease Transgenic Mice. *Neuron 30*, 665−676.

(16) Cherny, R. A., Atwood, C. S., Xilinas, M. E., Gray, D. N., Jones, W. D., McLean, C. A., Barnham, K. J., Volitakis, I., Fraser, F. W., Kim, Y.-S., Huang, X., Goldstein, L. E., Moir, R. D., Lim, J. T., Beyreuther, K., Zheng, H., Tanzi, R. E., Masters, C. L., and Bush, A. I. (2001) Treatment with a Copper-Zinc Chelator Markedly and Rapidly Inhibits β-Amyloid Accumulation in Alzheimer's Disease Transgenic Mice. *Neuron 30*, 665−676.

(17) Lee, J. Y., Friedman, J. E., Angel, I., Kozak, A., and Koh, J. Y. (2004) The Lipophilic Metal Chelator DP-109 Reduces Amyloid Pathology in Brains of Human Beta-Amyloid Precursor Protein Transgenic Mice. *Neurobio.l Aging 25*, 1315−1321.

(18) Adlard, P. A., Cherny, R. A., Finkelstein, D. I., Gautier, E., Robb, E., Cortes, M., Volitakis, I., Liu, X., Smith, J. P., Perez, K., Laughton, K., Li, Q. X., Charman, S. A., Nicolazzo, J. A., Wilkins, S., Deleva, K., Lynch, T., Kok, G., Ritchie, C. W., Tanzi, R. E., Cappai, R., Masters, C.

DOI: 10.1021/acschemneuro.5b00055
ACS Chem. Neurosci. 2015, 6, 535−541

L., Barnham, K. J., and Bush, A. I. (2008) Rapid Restoration of Cognition in Alzheimer's Transgenic Mice with 8-Hydroxy Quinoline Analogs Is Associated with Decreased Interstitial Abeta. *Neuron 59*, 43−55.
(19) Lannfelt, L., Blennow, K., Zetterberg, H., Batsman, S., Ames, D., Harrison, J., Masters, C. L., Targum, S., Bush, A. I., Murdoch, R., Wilson, J., and Ritchie, C. W. (2008) Safety, Efficacy, and Biomarker Findings of PBT2 in Targeting Abeta as a Modifying Therapy for Alzheimer's Disease: A Phase IIa, Double-Blind, Randomised, Placebo-Controlled Trial. *Lancet Neurol. 7*, 779−786.
(20) Faux, N. G., Ritchie, C. W., Gunn, A., Rembach, A., Tsatsanis, A., Bedo, J., Harrison, J., Lannfelt, L., Blennow, K., Zetterberg, H., Ingelsson, M., Masters, C. L., Tanzi, R. E., Cummings, J. L., Herd, C. M., and Bush, A. I. (2010) PBT2 Rapidly Improves Cognition in Alzheimer's Disease: Additional Phase II Analyses. *J. Alzheimer's Dis 20*, 509−516.
(21) Bareggi, S. R., and Cornelli, U. (2012) Clioquinol: Review of its Mechanisms of Action and Clinical Uses in Neurodegenerative Disorders. *CNS Neurosci. Ther. 18*, 41−46.
(22) Papazian, V., Jackson, T., Pham, T., Liu, X., Greguric, I., Loc'h, C., Rowe, C., Villemagne, V., Masters, C. L., and Katsifis, A. (2005) The Preparation of 123/125I-Clioquinol for the Study of Aβ Protein in Alzheimer's Disease. *J. Labelled Compd. Radiopharm. 48*, 473−484.
(23) Opazo, C., Luza, S., Villemagne, V. L., Volitakis, I., Rowe, C., Barnham, K. J., Strozyk, D., Masters, C. L., Cherny, R. A., and Bush, A. I. (2006) Radioiodinated Clioquinol As a Biomarker for β-Amyloid: Zn^{2+} Complexes in Alzheimer's Disease. *Aging Cell 5*, 69−79.
(24) Vasdev, N., Cao, P., van Oosten, E. M., Wilson, A. A., Houle, S., Hao, G., Sun, X., Slavine, N., Alhasan, M., Antich, P. P., Bonte, F. J., and Kulkarni, P. (2012) Synthesis and PET Imaging Studies of [18F] 2-Fluoroquinolin-8-ol ([18F]CABS13) in Transgenic Mouse Models of Alzheimer's Disease. *Med. Chem. Commum. 3*, 1228−1230.
(25) Cary, B. P., Brooks, A. F., Fawaz, M. V., Shao, X., Desmond, T. J., Carpenter, G. M., Sherman, P., Quesada, C. A., Albin, R. L., and Scott, P. J. H. (2015) Targeting Metal-Aβ Aggregates with Bifunctional Radioligand [^{11}C]L2-b and a Fluorine-18 Analogue [^{18}F]FL2-b. *ACS Med. Chem. Lett. 6*, 112−116.
(26) Lim, S., Paterson, B. M., Fodero-Tavoletti, M. T., O'Keefe, G. J., Cappai, R., Barnham, K. J., Villemagne, V. L., and Donnelly, P. S. (2010) A copper Radiopharmaceutical for Diagnostic Imaging of Alzheimer's Disease: A Bis(thiosemicarbazonato)copper(II) Complex That Binds to Amyloid-β Plaques. *Chem. Commun. 46*, 5437−5439.
(27) Hickey, J. L., Lim, S., Hayne, D. J., Paterson, B. M., White, J. M., Villemagne, V. L., Roselt, P., Binns, D., Cullinane, C., Jeffery, C. M., Price, R. I., Barnham, K. J., and Donnelly, P. S. (2013) Diagnostic Imaging Agents for Alzheimer's Disease: Copper Radiopharmaceuticals that Target Aβ Plaques. *J. Am. Chem. Soc. 135*, 16120−16132.
(28) Liang, S. H., Collier, T. L., Rotstein, B. H., Lewis, R., Steck, M., and Vasdev, N. (2013) Rapid Microfluidic Flow Hydrogenation for Reduction or Deprotection of 18F-Labeled Compounds. *Chem. Commun. 49*, 8755−8757.
(29) Rotstein, B. H., Stephenson, N. A., Vasdev, N., and Liang, S. H. (2014) Spirocyclic Hypervalent Iodine(III)-Mediated Radiofluorination of Non-Activated and Hindered Aromatics. *Nat. Commun. 5*, 4365.

DOI: 10.1021/acschemneuro.5b00055
ACS Chem. Neurosci. 2015, 6, 535−541